The Role of an Alkyl–Phenyl Spacer on the Reactivity of Novel Platinum(II) Complexes with Thiourea Nucleophiles

WANGOLI PANYAKO ASMAN

School of Chemistry and Physics, University of KwaZulu-Natal, 3209, Scottsville, Pietermaritzburg, South Africa

Received 24 December 2016; revised 21 January 2017; accepted 23 January 2017

DOI 10.1002/kin.21085
Published online in Wiley Online Library (wileyonlinelibrary.com).

ABSTRACT: The presented work, submitted as a paper, deals with the substitution reactions of mononuclear and dinuclear platinum(II) complexes of di-2-pyridylaminodiaquaplatinum(II), (**Pt1**); di-2-pyridylaminomethylbenzenediaquaplatinum(II), (**Pt2**); 1,2-bis(di-2-pyridylaminomethyl)benzenetetraquaplatinum(II), (**Pt3**); 1,3-bis(di-2-pyridylaminomethyl)benzenetetraquaplatinum(II), (**Pt4**); and 1,4-bis(di-2-pyridylaminomethyl)-benzenetetraquaplatinum(II), (**Pt5**). These reactions were carried out on aqua complexes by three nucleophiles, viz., thiourea, N,N′-dimethylthiourea, and N,N,N′N′-tetramethylthiourea under pseudo–first-order conditions as a function of nucleophile concentration and temperature by stopped-flow and UV–visible spectrophotometric techniques. In addition, some DFT calculation was performed. The activation parameters support an associative substitution mechanism. © 2017 Wiley Periodicals, Inc. Int J Chem Kinet 1–17, 2017

INTRODUCTION

Ligand substitutions on square-planar platinum(II) complexes have attracted continued attention owing to their intrinsic chemical and biomedical applications in antitumor treatment [1–3]. The interaction of these platinum-based drugs with deoxyribonucleic acid (DNA) is widely accepted as the mechanism responsible for their anticancer activity [4–6]. This has led to the need of understanding their chemical and the biomedical transformations under physiological conditions. To achieve this, many aspects of substitution reactions on monofunctional Pt(II) complexes have been carried out [7,8]. The results reported on substitution reactions of these monofunctional Pt(II) complexes mostly suggest an associative mechanism [9,10], although in some cases dissociative mechanisms have also been reported [11]. Despite the side effects of this class of complexes, they have been widely used as anticancer therapeutics. However, their limitations have led to considerable interest in the development

Correspondence to: W. P. Asman; e-mail: pwangoli@yahoo.com.
Supporting Information is available in the online issue at www.wileyonlinelibrary.com.

of multinuclear platinum(II) complexes as a promising class of new anticancer drugs [12,14]. These multinuclear complexes have shown potential antitumor activity and are reported to circumvent cisplatin resistance cell lines [1,2,5,6,13]. Recent reports in this area demonstrate a bright prospect in the utilization of multinuclear metal complexes in cancer chemotherapy [4,5].

Despite the advantages of these multinuclear platinum complexes, extensive study has been with regard to cisplatin which is reported to be among the most active antitumor agents in clinical use [15,16]. Cisplatin being among the mainstays in cancer chemotherapy has contributed to more detailed studies of monofunctional platinum(II) complexes. However, its narrow spectrum of activity and side effects [17,18] has led to many different and creative approaches toward the design of new classes of platinum-based complexes that address the side effects associated with cisplatin. One way of exploring this has been a paradigm shift from the mononuclear to multinuclear platinum complexes that may form different intrastrand and interstrand cross-link DNA-adducts with an expanded spectrum of activity [19–21]. The multinuclear complexes have shown pharmaceutical significance, for instance the advancement BBR3464 to clinical trials, and exhibiting antitumor activity in both cisplatin-sensitive and resistant cell lines [22,23].

Collectively, this class of complexes has been reported to display novel mechanisms of action over classical mononuclear complexes such as cisplatin and its analogues. Results from recent studies by Jaganyi et al. [24], Hofmann and van Eldik [25], and Farrell et al. [26] have reported the reactivity of dinuclear platinum(II) complexes to vary with the bridging linker that connects the two platinum centers. However, the actual thermodynamic or kinetic contribution of the bridge to the mechanism of substitution remains to be elucidated. Moreover, the molecular geometry, symmetry, and steric or electronic connotations adopted by the complexes remain unexplored. Variation in substitution rates by changing the bridging spacer and introduction of more bifunctional platinum centers remain a promising strategy in tuning platinum anticancer agents with improved efficacy [4–6].

The current study has been undertaken to investigate the role of alkyl–phenyl spacer on the multiple substitutions of the complexes with bidentate N^N donors of the form $[Pt(N^N)X_2]^{2+}$ with biological nucleophiles. The reaction of these complexes with *cis*-$PtCl_2$ configuration mimics the mechanism of cisplatin. In this paper, dinuclear complexes with configuration $[Pt(N^N)X_2Pt(N^N)X_2]^{4+}$ were formed by varying the connectivity of the alkyl spacer on the phenyl ring in ortho, meta, and para positions. The investigation reveals for the first time information on substitution mechanisms of transition metal complexes with multidentate ligands ($4H_2O$) as leaving groups in cis coordination. This study was motivated by the fact that dinuclear platinum(II) complexes have been reported to be promising anticancer agents owing to their formation of long-range intrastrand and interstrand cross-link DNA adducts [16,18]. The adducts are not common in mononuclear platinum(II) complexes, thus making their mechanism the center of focus.

In the current study, the 2,2-dipyridylamine ligand was used due to its unique coordination that forms six-membered chelates upon binding to the metal center and the ability of nitrogen donor ligands to stabilize both low and high oxidation states of complexes [29,30]. The current study explores how symmetry, geometry, electronic, steric as well as nucleophilic strength influences the rates of such substitution reactions. Thiourea nucleophiles were employed due to their differences in nucleophilicity, steric hindrance, and their biological relevance. For instance, thiourea (TU) is a strong σ-donor with high solubility and can act as a good model compound for thiolate and thioether present in the cells [31] and as a protecting agent to minimize nephrotoxicity in cisplatin treatment [4]. It is also known to act as a chemoprotective agent that alleviates the side effects in the normal tissue [4]. While *N,N′*-dimethylthiourea (DMTU) a highly permeate molecule, decreases injury in a wide variety of biological systems and inactivates reactive oxygen species [32,33]. It is envisaged that the kinetic tuning of the dinuclear complexes in Scheme 1 will shed light on their mechanistic interaction with biological molecules and provide a better understanding of their metabolism.

EXPERIMENTAL

Materials and Reagents

The nucleophiles TU (99%), DMTU (99%), *N,N,N′N′*-tetramethylthiourea (TMTU; 98%), 2,2-dipyridylamine (99%), benzyl bromide (99%), 1,2-bis(bromomethyl)benzene (99%), 1,3-bis(bromomethyl)benzene (99%), 1,4-bis(bromomethyl)benzene (99%), and $AgClO_4$ (99.99%) were all obtained from Sigma Aldrich. Potassium tetrachloroplatinate (K_2PtCl_4) was obtained from Strem chemicals. Ultrapure deionized water was used in all experiments. All other reagents were of analytical grade and used without further purification.

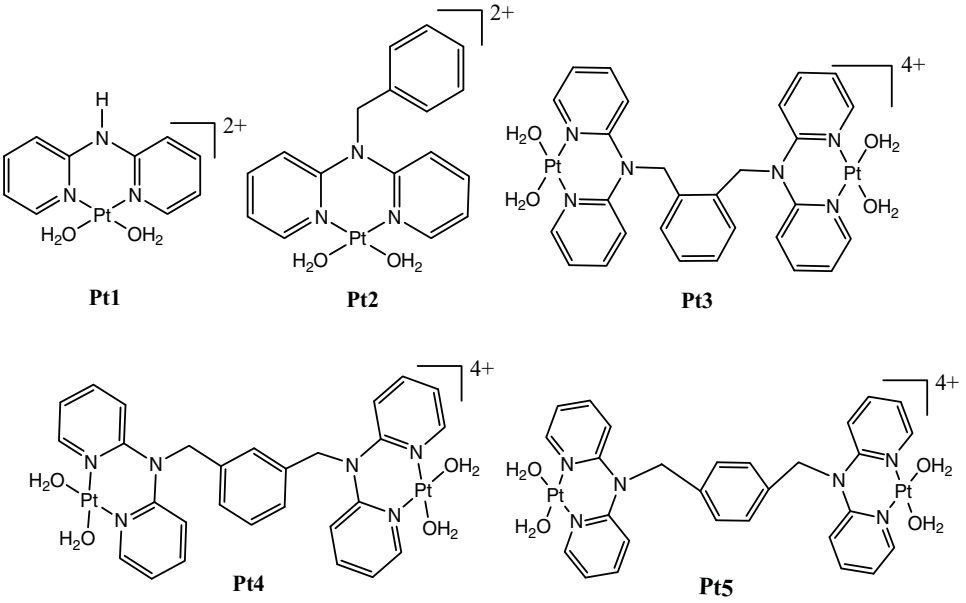

Scheme 1 Schematic structures and abbreviations for the Pt(II) complexes.

Synthesis of Ligands

Syntheses of ligands were carried out using the standard Schlenkline procedures under dry nitrogen. The ligands, namely di-2-pyridylaminomethylbenzene, 1,2-bis(di-2-pyridylaminomethyl)benzene, 1,3-bis(di-2-pyridylaminomethyl)benzene, and 1,4-bis(di-2-pyridylaminomethyl)benzene, were prepared according to the literature procedure [34], starting with 2,2′-dipyridylamine and their respective bromo alkyl halide linkers. For each ligand, the respective bromoalkyl halide (0.855 g, 5.00 mmol) was dissolved in 3 mL DMF at room temperature and 2,2′-dipyridylamine (0.856 g, 5.00 mmol) and KOH (1.137 g, 20.26 mmol) in 5.00 mL DMF was added dropwise. The resulting solution was stirred under nitrogen at room temperature for 24 h and then dried under in vacuo. The residue was washed with water and extracted with $CHCl_3$ (3 × 50 mL), and the extracts dried over anhydrous sodium sulfate and filtered. The filtrate was taken to dryness under reduced pressure. The residue was chromatographed on silica gel by elution with $CHCl_3$:CH_3OH (5:1). The resulting yellow product was recrystallized from an acetone–water mixture (1:2 v/v). However, synthesis of 1,2-bis(di-2-bromomethyl)benzene was carried out in DMSO and recrystallized in ethyl acetate–petroleum ether.

Di-2-pyridylaminomethylbenzene. Yield, 0.277 g, (21%). Anal. Calcd. for $C_{17}H_{15}N_3$, C, 78.13; H, 5.79; N, 16.08; Found: C, 77.78; H, 5.55; N, 16.48. ^{1}H NMR (400 MHz, $CDCl_3$, 303 K) δ 8.40 (2H, d, py), 7.60 (2H, t, py), 7.37 (2H, d, py), 7.27 (2H, d, ph), 7.20 (1H, t, ph), 7.16 (2H, d, ph), 6.94 (2H, t, py), 5.55 (2H, s, CH_2); ^{13}C NMR (400 MHz, $CDCl_3$, 303 K) δ 157.5, 148.6, 139.8, 137.4, 128.0, 117.4, 114.4, 51.3, TOF MS ES$^+$, *m/z*: 262.134 $[M + H]^+$.

1,2-Bis(di-2-pyridylaminomethyl)benzene. Yield, 0.369 g, (37%). Anal. Calcd. for $C_{28}H_{24}N_6$, C, 75.65; H, 5.44; N, 18.91; Found C, 75.39; H, 5.27; N, 19.28. ^{1}H NMR (400 MHz, $CDCl_3$, 303 K) δ 8.32 (4H, d, py), 7.53 (4H, t, py), 7.27 (2H, d, ph), 7.22 (4H, d, py), 7.04 (2H, t, ph), 6.86 (4H, dd, py), 5.64 (4H, s, CH_2); ^{13}C NMR (400 MHz, $CDCl_3$, 303 K) δ 157.1, 148.2, 137.3, 136.4, 127.6, 126.4, 117.3, 114.6, 48.3, TOF MS ES$^+$, *m/z*: 445.2141 $[M + H]^+$.

1,3-Bis(di-2-pyridylaminomethyl)benzene. Yield, 0.463 g, (46%). Anal. Calcd. for $C_{28}H_{24}N_6$, C, 75.65; H, 5.44; N, 18.91; Found C, 75.75; H, 5.36; N, 19.19. ^{1}H NMR (400 MHz, $CDCl_3$, 303 K) δ 8.25 (4H, d, py), 7.53 (4H, t, py), 7.27 (2H, d, ph), 7.22 (4H, d, py), 7.04 (2H, t, py), 6.86 (4H, t, py), 5.64 (4H, s, CH_2); ^{13}C NMR (400 MHz, $CDCl_3$, 303 K) δ 157.1, 148.1, 139.6, 136.9, 128.4, 125.0, 114.3, 51.1, TOF MS ES$^+$, *m/z*: 445.2136 $[M + H]^+$.

1,4-Bis(di-2-pyridylaminomethyl)benzene. Yield, 0.599 g, (59%). Anal. Calcd. for $C_{28}H_{24}N_6$, C, 75.65; H, 5.44; N, 18.91; Found C, 75.57; H, 5.32; N, 19.27. ^{1}H NMR (400 MHz, $CDCl_3$, 303 K) δ 8.28 (4H, d, py), 7.47 (4H, t, Py), 7.22 (4H, s, ph), 7.13 (4H, d, py), 6.82 (4H, dd, py), 5.43 (4H, s, CH_2); ^{13}C NMR (400 MHz, $CDCl_3$, 303 K) δ 157.1, 148.1, 137.6, 137.1,

126.9, 117.1, 114.5, 51.0, TOF MS ES$^+$, *m/z*: 467.1957 $[M + Na]^+$.

Syntheses of Complexes

The complexes were synthesized from their respective ligands according to the literature method by Krebs et al. [35] A 50-mL solution of K_2PtCl_4 was stirred, and the corresponding molar equivalent of respective ligands dissolved in a small amount of water was added dropwise. The reaction mixture was refluxed overnight at 50°C. The resulting platinum(II) complexes were obtained as precipitates, washed with ultrapure water and diethyl ether, and finally dried in vacuo. The synthesized ligands and complexes were characterized using $^1H-^{13}C$ and ^{195}Pt NMR, mass spectrometry and elemental analysis.

Pt1. Yield, 66 mg, (63%), yellow powder. Anal. Calcd. for $C_{10}H_9N_3PtCl_2$, C, 27.54; H, 2.08; N, 9.64; Found C, 27.36; H, 2.29; N, 9.16. ^1H NMR (400 MHz, DMSO-d_6, 303 K), 8.80 (2H, d, py), 7.98 (2H, t, py), 7.27 (2H, d, py), 7.14 (2H, t, py), 4.04 (1H, s, N─H), ^{13}C NMR (400 MHz, DMSO-d_6, 303 K), 170.8., 150.4, 141.0, 119.4, 114.3, 60.1, TOF MS ES$^+$, *m/z*: 437.9808, ^{195}Pt NMR –2103.4 ppm.

Pt2. Yield, 69 mg, (44%). Anal. Calcd. for $C_{17}H_{15}N_3PtCl_2$, C, 38.72; H, 2.87; N, 7.97; Found C, 38.46; H, 3.07; N, 8.10. ^1H NMR (400 MHz, DMSO-d_6, 303 K), 9.05 (2H, d, py), 8.04 (2H, t, py), 7.68 (2H, d, py), 7.53 (2H, d, py), 7.36 (2H, t, py), 7.26 (5H, d, ph), 5.43 (2H, s, CH_2); ^{13}C NMR (400 MHz, DMSO-d_6, 303 K): 153.8, 151.8, 142.1, 136.3, 129.8, 122.1, 117.4, 54.3, TOF MS ES$^+$, *m/z*: 550.0247 $[M + Na]^+$, ^{195}Pt NMR –2189.2 ppm.

Pt3. Yield, 75 mg (0.08 mmol) (36%). Anal. Calcd. for $C_{28}H_{24}N_6Pt_2Cl_4$, C, 34.45, H, 2.48, N, 8.61; Found C, 34.32, H, 2.52, N, 8.56. ^1H NMR (400 MHz, DMSO-d_6, 303 K), 8.83 (2H, d, py), 8.20 (2H, t, py), 7.96 (2H, d, py), 7.56 (4H, d, py), 7.44 (2H, t, py), 7.26 (4H, d, py), 7.02 (2H, t, ph), 6.92 (2H, d, ph), 5.38 (4H, s, CH_2), ^{13}C NMR (400 MHz, DMSO-d_6, 303 K): 157.2, 153.4, 148.6, 138.2, 125.4, 117.6, 113.7, 51.0, TOF MS ES$^+$, *m/z*: 941.05 $[M–Cl]^+$, ^{195}Pt NMR –2187.3 ppm.

Pt4. Yield, 92 mg (0.10 mmol) (44%). Anal. Calcd. for $C_{28}H_{24}N_6Pt_2Cl_4$, C, 34.45, H, 2.48, N, 8.61; Found C, 34.32, H, 2.52, N, 8.56. ^1H NMR (400 MHz, DMSO-d_6, 303 K), 8.83 (2H, t, py), 8.22 (2H, d, py), 8.02 (3H, d, py), 7.58 (4H, d, py), 7.44 (3H, d, py), 7.28 (4H, d, ph), 7.02 (2H, d, py), 5.39 (4H, s, CH_2); ^{13}C NMR (400 MHz, DMSO-d_6, 303 K): 157.1, 148.8, 138.6, 114.2, 111.3, 54.5, TOF MS ES$^+$, *m/z*: 941.04 $[M – Cl].^+$ ^{195}Pt NMR –2190.6 ppm.

Pt5. Yield, 106 mg (0.11 mmol) (51%). Anal. Calcd. for $C_{28}H_{24}N_6Pt_2Cl_4$, C, 34.45, H, 2.48, N, 8.61; Found C, 34.23, H, 2.34, N, 8.26. ^1H NMR (400 MHz, DMSO-d_6, 303 K), 8.28 (4H, d, py), 7.63 (4H, t, py), 7.19 (8H, s, py), 6.94 (4H, d, ph), 5.35 (4H, s, CH_2), ^{13}C NMR (400 MHz, DMSO-d_6, 303 K): 157.6, 147.9, 137.6, 127.3, 117.6, 115.0, 50.4, TOF MS ES$^+$, *m/z*: 941.05 $[M – Cl]^+$. ^{195}Pt NMR –2194.8 ppm.

Aquation of Chloro Complexes

Owing to the low solubility of the chloro complexes, the complexes were converted to their aqua analogues according to Bugarčić et al. [36] procedure. The aqua solutions were prepared from their corresponding chloro complexes by removing the chloride ion using $AgClO_4$. An almost stoichiometric amount of $AgClO_4$ was added to the solution and refluxed for 24 h at 50°C in the dark. The white AgCl precipitate that formed was removed by filtration through a 0.45-μm pore membrane filter. This was to ensure complete conversion to aqua and removal of silver ions. The aqua solutions were made to the required concentration using a solution of 0.1 M $HClO_4$ acid. The use of acidic solutions of pH 1.0 ensured that complex solutions are in the aqua form and maintained a constant ionic strength of 0.1 M. This ensured that pK_a values were determined at similar ionic strength. The aqua solutions were titrated with NaOH solution to determine the pK_a of the complexes. While for all kinetic studies, a pH of 2.0 and an ionic strength at 0.1 M using $NaClO_4$ was maintained to minimize effects of ionic strength.

Physical Measurements

Characterization of both the ligands and complexes using ^1H, $^{13}C'$, and ^{195}Pt NMR spectroscopy was recorded on a Bruker Avance III 500 or Bruker Avance 400 spectrometers at frequencies of 500 or 400 MHz and 125 MHz/100 MHz using either a 5-mm BBOZ probe or a 5-mm TBIZ probe. All proton and carbon shifts were recorded with reference to the relevant solvent signal used. Chemical shift values are given in δ (ppm) of ^1H relative to tetramethylsilane ($Si(CH_3)_4$), whereas ^{195}Pt was externally referenced to $K_2[PtCl_6]$ in D_2O. For mass determination, a Waters Micro-mass LCT Premier spectrometer was employed. Elemental analysis was obtained on a Thermo Scientific Flash 2000. Kinetic studies for fast reactions were monitored using an Applied Photophysics SX20 stopped-flow spectrophotometer coupled to an online data acquisition system, whereas a Varian Cary 100 Bio UV–visible spectrophotometer thermostated by a Varian

Peltier temperature controller to within ±0.05°C was used for the slow kinetic measurements. The kinetic traces were analyzed using the Origin 7.5® software package [37]. The pH of the solutions was recorded on a Jenway 4330 conductivity/pH meter. Standard pH calibration buffer solutions (pH 4.0, 7.0, and 10.0) were used for calibration.

pK_a Determination of the Aqua Complexes

To obtain the intrinsic information on the acidity of the complexes and their effect on reactivity, their pK_a values were determined. UV–vis spectra for the determination of pK_a values were recorded on a Varian Cary 100 Biospectrophotometer. NaOH was used as the base for spectrophotometric titration in the pH range 1–10. To avoid absorbance corrections due to dilution, a large volume of the platinum aqua complex (250 mL) was used. Solid NaOH pellets were used initially in the pH range of 1–3 after which the Pasteur pipettes were used for dropwise addition of 0.5, 0.1, 0.05, and 0.001 M of NaOH solution and similar concentrations for perchloric acid for adjusting the pH.

Kinetic Measurements

Substitution reactions were performed at pH 2.0, where the complexes exist in their aqua form (as predetermined when determining pK_a) and protonation of TU nucleophiles ruled out [38]. The rate of substitution of the aqua complexes was determined under pseudo–first-order conditions as a function of nucleophile concentration and temperature using stopped flow for fast and UV–vis spectroscopy for slow reactions by following the change in absorbance at suitable wavelengths (Table S1 in the Supporting Information). All the kinetic runs were fitted by a single exponential to determine the k_{obs}. The activation parameters of enthalpy ($\Delta H^{\#}$) and entropy($\Delta S^{\#}$)were obtained by varying the temperature between 288 and 313 K at an interval of 5 K. These parameters were calculated from Eyring plots using Eq. (1):

$$In\left(\frac{k_2}{T}\right) = -\frac{\Delta H^{\#}}{RT} + \left[In\left(\frac{k_B}{h}\right)\right] + \frac{\Delta S^{\#}}{R} = \frac{\Delta H^{\#}}{RT} + \left(23.8 + \frac{\Delta S^{\#}}{R}\right) \quad (1)$$

where k_B and h are Boltzmann's and Planck's constants, respectively, whereas R is a gas constant and T is absolute temperature.

Computational Calculations

Density functional theory (DFT) calculations were performed with the Gaussian 09 program suite [39]. Geometrical optimizations were carried at B3LYP/LanL2DZ level of theory. B3LYP refers to a three-parameter functional hybrid exchange of Becke [40] with functional correlation gradient of Lee et al. [40], whereas LanL2DZ refers to Los Alamos National Laboratory 2 Double ζ basis set [40]. The singlet states were used due to low electronic spin of Pt(II) complexes. The aqua complexes were modeled as cations of overall charge +2 for mononuclear and +4 for dinuclear. The DFT provided the ground state properties of the systems and the electron density. Molecular orbital calculations were performed to give HOMO and LUMO energies using LanL2DZ/B3LYP basis set.

RESULTS AND DISCUSSION

pK_a Determinations for the Aqua Pt(II) Complexes

To ascertain the pK_a values of the complexes, a titration study was undertaken. Figure 1 show a typical UV–vis spectrum recorded during spectrophotometric titration of the aqua complex solution with NaOH. To determine pK_a values, absorbance was measured as a function of pH. This resulted in a characteristic sigmoid curve from which the pK_a was determined by locating the inflection point (Figs. S39 and S40 in the Supporting Information).

The study shows the nature and conformation of the spacer in the dinuclear complexes to have little influence on the pK_a values as they are of similar magnitude. The ortho/para orientation effect of the alkyl substituent has a natural consequence of the preferential stabilizing influence as exhibited in this investigation. The effect depends on the position of the alkyl group, which exhibits stronger electron-donating effect in the para position than ortho and meta positions [41a–c]. The only difference among these three complexes is the position of the alkyl group on the phenyl group. The study notes that the slight change in the anchorage position results in a significant difference in their chemical structure, pK_a values, and reactivity. This investigation shows that alkyl group's electron-donating effect in ortho/para is stronger than in the meta position. This is supported by computational calculations (Table III) showing varying bond angles of $C_1N_3C_2$ Pt5 (123.07°) > Pt3 (122.72°) > Pt4 (118.55°), representing para > ortho > meta, respectively. Thus, the meta complex is more acidic since it only has inductive

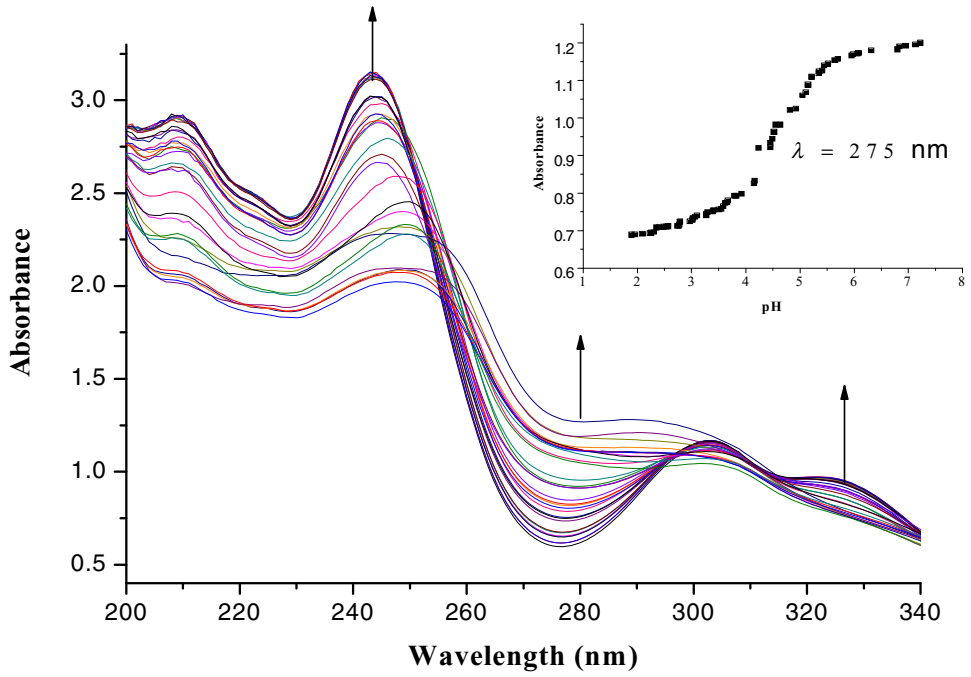

Figure 1 UV–vis spectra of **Pt1** complex recorded as a function of pH in the range of 2–8 at *25°C; inset is a plot of absorbance versus pH at* $\lambda = 275$ *nm.* [Color figure can be viewed at wileyonlinelibrary.com]

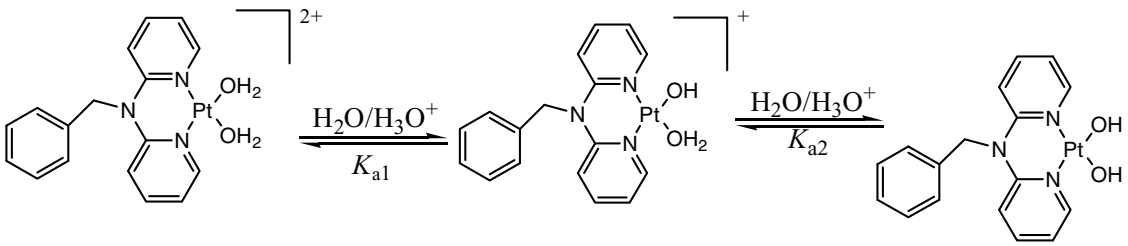

Scheme 2 Proposed mechanism for stepwise deprotonation of the diaqua Pt(II) mononuclear complex.

effects, whereas the ortho/para complexes experience both inductive and resonance effects. This investigation shows the ortho/para orientation effect of the alkyl substituent has a natural preferential stabilizing effect. The study shows that substituents' position has an influence on the stability of a complex through both electronic and steric effects. Thus, by having alkyl substituents at ortho and para positions behave identically but different from that of meta position. As such, one would expect the meta complex to have a significantly different pK_a value as observed in this investigation.

The acidity of complexes shows that the dinuclear complexes are slightly more acidic using first deprotonation for comparison. This difference can be ascribed to the difference in the overall charge of the complexes which is +2 for the mononuclear and +4 for the dinuclear complexes. Coordination of a second Pt(II) atom results in addition of charges that make the dinuclear platinum complexes more electrophilic thus favouring aqua deprotonation. The results also show that the deprotonation of the subsequent water molecules occurs at higher pH values. This is due to the sequential reduction of the overall charge after each deprotonation, which results in the Pt(II) center of the aqua/hydroxo species being less electrophilic [8,25] leading to higher pK_a values. Complex Pt1 showed three pK_a values, which are attributed to the two aqua ligands and the pendant acidic proton on N. The proposed deprotonation process can therefore be represented by the equilibrium reaction given in Scheme 2 whereas the pK_a values are summarized in Table I. The results support a stepwise deprotonation. This investigation shows similar behavior in deprotonation process to previous study by van Eldik [36d] and group on dinuclear Pt(II)

Table I A Summary of pK_a Values Obtained for Stepwise Deprotonation of Aqua Pt(II) Complexes Investigated

Complex	Pt1	Pt2	Pt3	Pt4	Pt5
pK_{a1}	2.72 ± 0.06	2.87 ± 0.02	2.55 ± 0.03	2.39 ± 0.01	2.61 ± 0.01
pK_{a2}	3.80 ± 0.02	6.97 ± 0.11	3.24 ± 0.03	3.65 ± 0.03	3.62 ± 0.01
pK_{a3}	5.68 ± 0.02		5.46 ± 0.02	4.41 ± 0.02	4.16 ± 0.03
pK_{a4}			7.37 ± 0.04	6.90 ± 0.08	7.43 ± 0.01

Boltzmann equation, $y = A_2+(A_1-A_2)/(1 + \exp((x-x_0)/dx)$, was used in determining the p*K*a values using the Origin 7.5® program (Figs. S39–S41 in the Supporting Information).

Table II The Optimized Structures of the Molecular Frontier Orbitals of the Studied Complexes at B3LYP/LanL2DZ Level of Theory (Iso Value = 0.02)

Complex	Planarity	HOMO Map	LUMO Map
Pt1	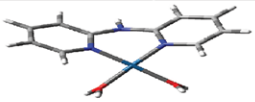	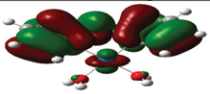	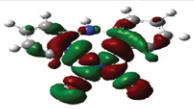
Pt2	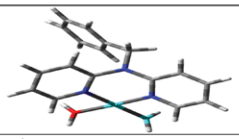	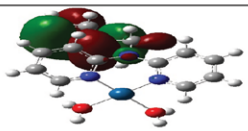	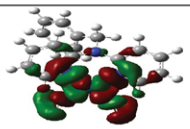
Pt3	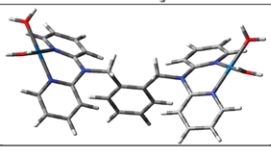	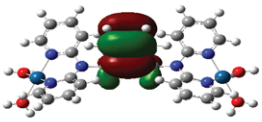	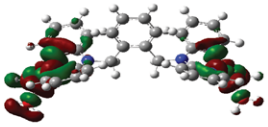
Pt4	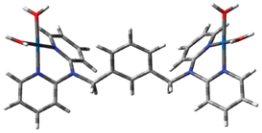	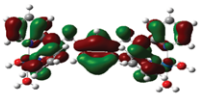	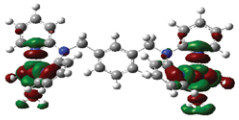
Pt5	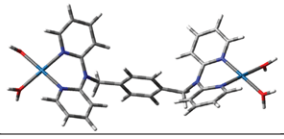	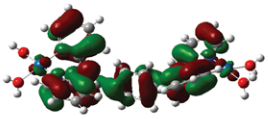	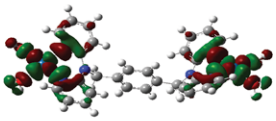

complexes coordinated to four aqua ligands that showed four acid dissociation steps. The two aqua ligands coordinated to each platinum center exhibited different pK_a values supporting recent study by Jaganyi and Kinunda using the same head group [41d]. This study shows dinuclear complexes to be more acidic than mononuclear analogues due to increased charge as reported in the literature [36].

Computational Studies

To gain further insight into the influence of the anchorage position of the alkyl–phenyl spacer on the conformation and possible kinetic properties of the complexes, computational studies were undertaken to determine the structural and electronic properties of the molecules. The complexes were fully optimized in gas phase, and their frontier molecular orbitals and selected geometrical parameters are summarized in Tables II and III respectively. To understand the extent of deviation from planarity, dihedral and basal angles were determined as shown in Fig. 2. The optimized structures show that the six-membered chelate rings containing the platinum adopt a twisted-boat conformation. The bond angles of the amine nitrogen are close to 120° an indication of sp^2 hybridized nitrogen atom [42a]. The introduction of the alkyl–phenyl spacer results in a conformation that is dependent on the position of the alkyl group on the phenyl, that form bowl like cavity. In the case of both ortho and meta

Table III A summary of selected DFT data for the investigated complexes

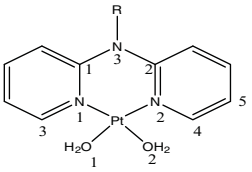

	Pt1	Pt2	Pt3	Pt4	Pt5
HOMO–LUMO energy					
LUMO (eV)	−9.18	−8.77	−11.64	−11.46	−11.33
HOMO (eV)	−13.20	−11.88	−15.82	−15.65	−15.53
ΔE (eV)	4.02	3.11	4.18	4.19	4.20
Electrophilicity index (ω)	31.15	34.20	45.10	43.78	43.41
NBO Charges					
Pt_1	0.766	0.760	0.770	0.766	0.771
Pt_2	–	–	0.770	0.766	0.771
N_1	−0.528	−0.518	−0.520	−0.516	−0.520
N_2	−0.528	−0.520	−0.520	−0.517	−0.521
N_3	−0.634	−0.508	−0.501	−0.509	−0.505
Dipole moment (Debye)	2.30	6.44	9.04	5.78	1.78
Bond length (Å)					
C_1–N_3	1.3979	1.4112	1.4189	1.4277	1.4140
C_2–N_3	1.3979	1.4091	1.4189	1.4182	1.4134
C_1–N_1	1.3688	1.3737	1.3751	1.3758	1.3751
C_2–N_2	1.3688	1.3737	1.3751	1.3728	1.3753
Pt–N_1	2.0099	2.0042	2.0039	2.0018	2.0045
Pt–N_2	2.0099	2.0041	2.0039	2.0018	2.0046
$Pt_1 \ldots Pt_2$			11.758	12.088	13.871
Bond angles (°)					
$C_1N_3C_2$	127.25	120.30	122.72	118.55	123.07
Dihedral angles	39.88	50.37	43.52	50.13	44.26
Basal angle	140.12	129.63	136.48	129.87	135.74

Where R = H, benzyl.

the boat conformation is not part of the cavity created between the two metal centers whereas in the para it is part of the cavity. In meta and para, the phenyl ring is positioned in the center of the cavity whereas in the ortho it is away from the cavity. These configurations introduce steric hindrance to the incoming nucleophile to different degrees. DFT calculations show that there is very little if any electronic effect when the pendant alkyl–phenyl is attached to Pt2 or used as a spacer in Pt3 to Pt5. Both the NBO charges and the electrophilicity index are similar in magnitude because of Pt(II) centers being in similar environment due to identical atomic and conjugative connectivity to at least five atoms in all directions. This is also supported by the HOMO–LUMO gap. The difference between the reactivity of monomers and the dinuclear complexes is attributed to the complex [42b]. One would therefore expect that the reactivity of these complexes to be controlled by the steric effect.

The study shows Pt(II) to be sensitive to the number of d electrons and their arrangement in the d orbitals. The strong σ donation from H^- in Pt1 shows HOMO orbitals to be localized on the pyridine rings and on the d orbitals of the metal. The negative charge built on the metal by strongly σ-donating –NH- moiety in Pt1 destabilizes the metal $d\pi$ orbitals thus lowering the $d\pi \rightarrow \pi^*$. This results from increased electron density on either a pyridine ring by conjugation with π electrons of the pyridine rings. The complex, Pt1, involves $5d_z{}^2$ orbitals which is the highest occupied molecular orbital and as a consequence strongly repels the incoming nucleophile compared to Pt2. As such there is a greater repulsive effect of $d_z{}^2$ than d_{xz}, d_{yz}, and d_{xy} orbitals because of its orientation to the entering ligand. On the contrary, the d_{xz}, d_{yz}, and d_{xy} orbitals are oriented away from the incoming ligands and are lower in energy. The greater electron transfer from H^- donor to the $5d_z{}^2$ orbitals of the platinum center destabilizes these orbitals than the d_{xz} and d_{yz} orbitals. This strong electron transfer to the acceptor pyridyl rings that fills $5d_z{}^2$ orbitals of metal center leads to higher

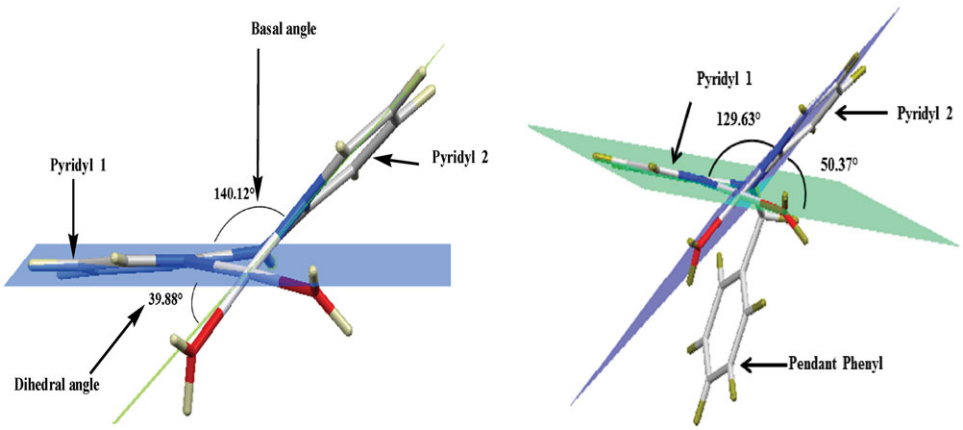

Figure 2 DFT-optimized structures of Pt1 and Pt2 showing dihedral and basal angles of the boat conformed pyridine rings. [Color figure can be viewed at wileyonlinelibrary.com]

stabilization energy of the Pt(II) center hence slow reactivity.

The study utilized the reactivity index (electrophilicity index, ω) to measure the stabilization in energy when the system acquires an additional electronic charge from the environment [43–49]. This value supports Pt2 (34.20 eV) to be more reactive than Pt1 (31.15 eV), which is in line with the experimental data. This difference in the electrophilicity values between the two complexes indicates a measure of energy lowering between the ligand systems due to maximal electron flow between the donor and acceptor. For changes in the ligand system, the dipole moments decrease in the order Pt2 (6.44 D) > Pt1 (2.30 D) which further corroborates with the reactivity of the two moieties showing Pt2 with higher dipole moment to have greater reactivity. However, the dinuclear isomers show no clear dipole moment trend in relation to reactivity as a consequence of different arrangement of substituents in ortho, meta, and para positions. As expected, the dipole moments followed the following order Pt3 (ortho) > Pt4 (meta) > Pt5 (para). The trend exhibits the electron density distribution in the complexes. However, this study shows dipole forces to have no significant influence on the reactivity of dinuclear complexes.

Kinetic Measurements

The kinetics of substitution of coordinated aqua ligands were investigated spectrophotometrically using conventional UV–vis and stopped flow techniques. A typical stopped-flow kinetic trace obtained is shown in Fig. 3, whereas Figs. 4 and 5 represent the typical UV–visible spectrophotometer kinetic traces. For each reaction, the values of k_{obs} were determined at five different concentrations of nucleophile [Nu]. The k_{obs} values were obtained from nonlinear least squares fit of the experimental data by fitting to Eq. (2) [9].

$$A_t = A_\infty + (A_0 - A_\infty)\exp^{(-k_{obs}t)} \quad (2)$$

where A_0, A_t, and A_∞ represent the absorbance of the reaction mixture initially, at time t, and at the end of the reaction, respectively. The second-order rate constant, k_2, for the reaction of each metal complex was obtained from the linear regression of the plots of k_{obs} versus nucleophile concentration using origin 7.5® [37]. Straight lines with zero or with negligible intercepts were obtained as presented in Figs. 6 and S1–S6 in the Supporting Information. A summary of k_2 values calculated at 25°C for the two steps are given in Table III and the corresponding rate law described by Eq. (3)

$$k_{obs(1/2)} = k_{-2} + k_{2(1st/2nd)}[Nu] \approx k_{2(1st/2nd)}[Nu] \quad (3)$$

where k_{-2} is a solvent path and is either zero or infinitesimal and k_2 is the second-order rate constant for a direct path. The two observed substitution steps are due to the simultaneous substitution of the water molecules followed by the dechelation of the linker as supported by the NMR study.

Activation Parameters

The activation parameters for the reactions were determined from the Eyring plots shown in Fig. 7 and in (Fig.s S7–S10 in the Supporting Information). The corresponding values for the activation parameters of Enthalpy, $\Delta H^{\#}$, and entropy, $\Delta S^{\#}$, are summarized in Table V. These results are temperature depentent and

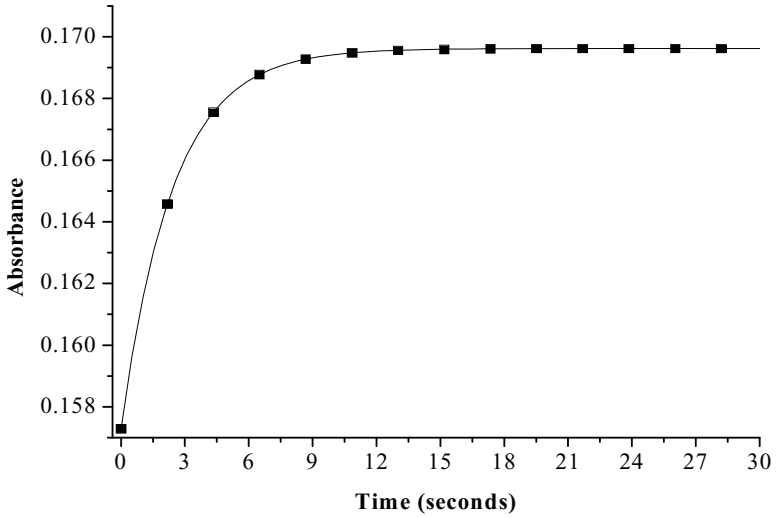

Figure 3 A typical kinetic trace showing a substitution step between Pt2 and TU at 290 nm, $T = 298.15$ K, pH 2.0, $I = 0.1$ M ($NaClO_4$) on the stopped-flow spectrophotometer.

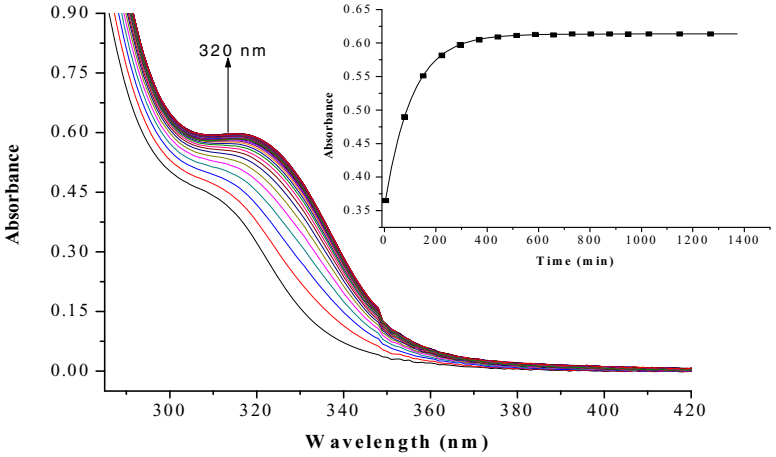

Figure 4 Absorbance spectra of Pt2 with TU; inset is a typical kinetic trace on the UV–visible spectrophotometer at 320 nm, $T = 298$ K, pH 2.0, and $I = 0.1$ M $NaClO_4$. [Color figure can be viewed at wileyonlinelibrary.com]

are in agreement with an associative substitution mechanism for square planar Pt(II) complexes based on the negative activation entropy values as reported in the literature [9,10,55].

Substitution Process

From the kinetic studies, the substitution proceeds via a two-step associative mechanism. The first step was attributed to simultaneous substitution of the labile aqua ligands at each platinum center. To confirm the second step as the displacement of the ligand, substitution reaction of complex Pt2 as a chloride with TU (6 equiv.) was monitored by ^{1}H NMR and ^{195}Pt NMR spectroscopy. Figures 8 and 9 show arrays of ^{1}H and ^{195}Pt NMR spectra, respectively. The pyridyl protons (H_a) were monitored due to their proximity to N-donor atoms coordinated to the metal center. The proton resonances of this unreacted chloro complex (Pt2) labeled H_a appear at $\delta = 9.05$ ppm and $\delta = -2189.2$ ppm on ^{1}H and ^{195}Pt NMR spectra, respectively. During the course of reaction, these resonances shift upfield to $\delta = 8.40$ ppm and $\delta = -3889.2$ ppm on ^{1}H and ^{195}Pt NMR, respectively. These shifts are attributed to the complexation between the metal and the ligand. This is because on coordination, the metal center pulls electron density from the pyridyl rings causing deshielding of protons to lower field as indicated by H_a in

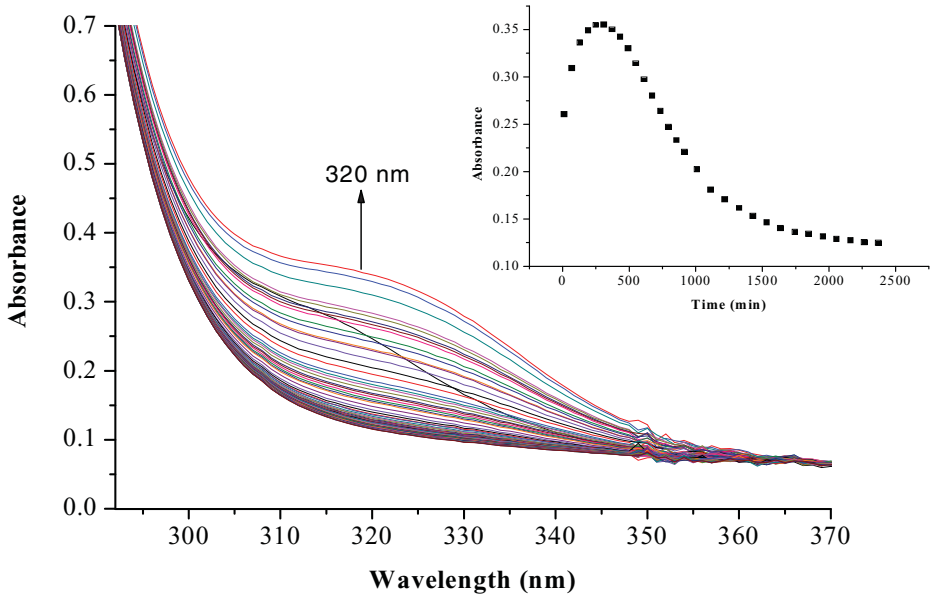

Figure 5 The time-resolved UV–vis absorption spectra of Pt5 with TU; inset is a kinetic trace for time dependence of absorbance at 320 nm showing a two-step reaction at $T = 298.15$ K, pH 2.0 and $I = 0.1$ M $NaClO_4$. [Color figure can be viewed at wileyonlinelibrary.com]

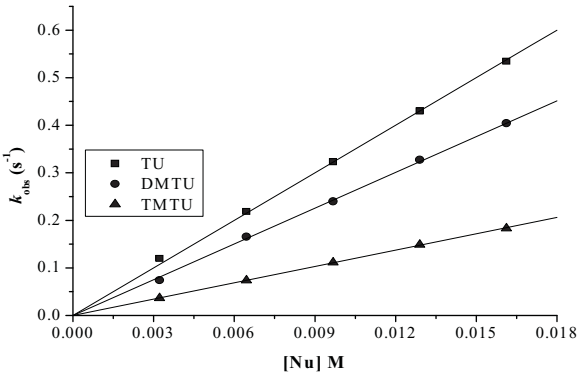

Figure 6 Concentration dependence of k_2 for the substitution of the simultaneous aqua ligands in Pt2 by nucleophiles at pH 2.0, $T = 298.15$ K, $I = 0.1$ M $NaClO_4$.

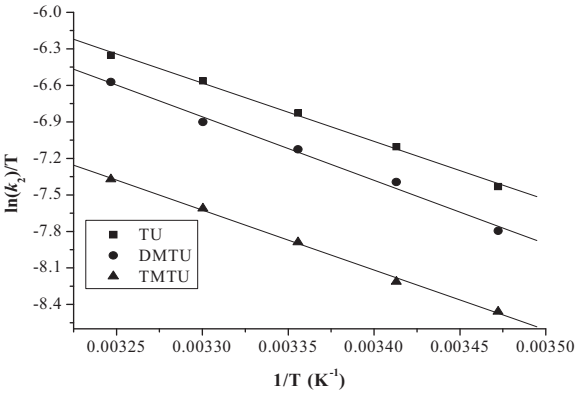

Figure 7 Eyring plots for the determination of the activation parameters for the aqua substitution of Pt2 with respective nucleophiles $I = 0.1$ M $NaClO_4$, pH 2.0.

Fig. 8. The H^1 and ^{195}Pt NMR confirms changes in electron distribution within the ligand–metal coordination sphere.

The peak at −2189.2 ppm on the ^{195}Pt NMR spectrum is indicative that the platinum is coordinated to two nitrogen atoms [50], whereas the peak at −3889.2 ppm in Fig. 9 shows the formation of the $Pt(TU)_4^{2+}$ complex [20] due to the excess TU displacing the ligand. The formation of the $Pt(TU)_4^{2+}$ complex supports the reaction mechanism proposed in Scheme 3. From these observations, it can be concluded that the second step is due to the displacement of the dipyridylamine ligand due to strong trans-effect of sulfur on coordination of TU to the Pt(II) center. These results are in accordance to the previous work reported on Pt(II) complexes of the type $[L_2PtX_2]$ where X = anionic leaving group; L = ammonia, amine, pyridine [51–53] Also studies on mononuclear dipyridylamine bidentate Pt(II) complexes appended to the alkyl flexible backbone recently reported by our group [41d] show similar behavior of this ligand head group to undergo dechelation process.

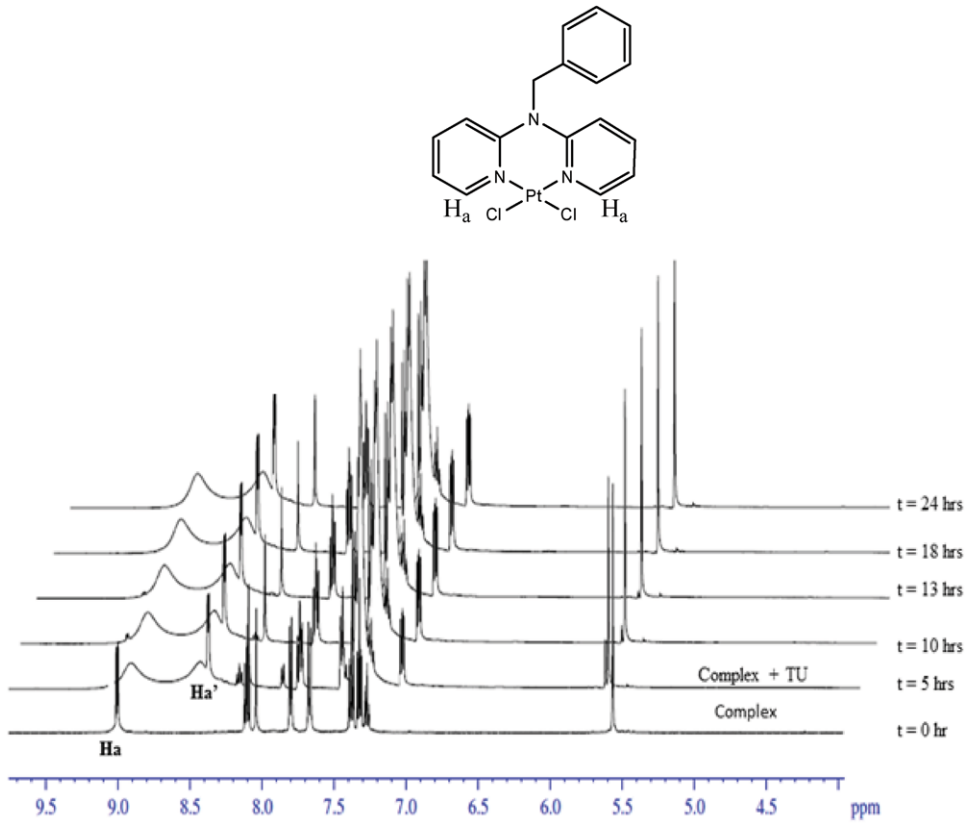

Figure 8 Time-dependent changes in the ^{1}H NMR spectra array of Pt2 upon addition of 6 equiv. of TU in DMF. The complex undergoes dechelation to form free ligand (starting material) after 24 h. [Color figure can be viewed at wileyonlinelibrary.com]

DISCUSSION

In this paper, the role of alkyl–phenyl moiety as a pendant and a spacer group on the reactivity Pt(II) complexes with multisubstitution of four aqua ligands with TU nucleophiles of different electronic and steric demands was investigated. The general reactivity in terms of k_2 values increased in the following order: Pt2 (33.34 M^{-1} s^{-1}) > Pt1 (28.85 M^{-1} s^{-1}) > Pt4 (0.16 M^{-1} s^{-1}) > Pt3 (0.08 M^{-1} s^{-1}) > Pt5 (0.04 M^{-1} s^{-1}) with TU as the entering nucleophile (Table IV). This observed reactivity trend is in line with the overall electrophilicity and the steric demands of the complexes.

The study shows that mononuclear Pt(II) complexes react faster than dinuclear analogues. This is in agreement with earlier findings by Adnan and Mika [54] who attributed the retardation to increased amount of steric demand in dinuclear Pt(II) complexes compared to mononuclear complexes. The steric effect is due to the "cage in-effect" as a result of the linker coordination position. The difference in reactivity between the two mononuclear complexes is attributed mostly to the electronic effect although there may be minor extent of steric factors. The slow reactivity of Pt1 is due to the stronger σ-donor property of H^- which increases electron density around the ligand system in comparison to the $-CH_2-$ group. The study shows a strong influence of the bridging moiety on the molecular and electronic properties of the complexes [55]. This is supported by DFT data in Table III, which shows a higher negative charge density (−0.634) on the amine nitrogen (N_3) in Pt1 compared to Pt2 with (−0.508). This is further supported by the electrophilicity index values and the short C_1-N_3 and C_2-N_3 bond lengths in Pt1 compared to Pt2. The stronger electron donation of H^- compared to $-CH_2-$ is also evident in the HOMO–LUMO energy gap (ΔE) difference between the two complexes. It is important to note that energy gap is an important stability index. The large gap of Pt1 (4.02 eV) compared to Pt2 (3.11 eV) implies high stability for this complex. The net result is a system that is more electronegative in Pt1 than in Pt2. In addition to the electronic effect is the entrapment of the nucleophile in the cavity created the two pyridine rings. The basal angle for Pt1 (140.12°)

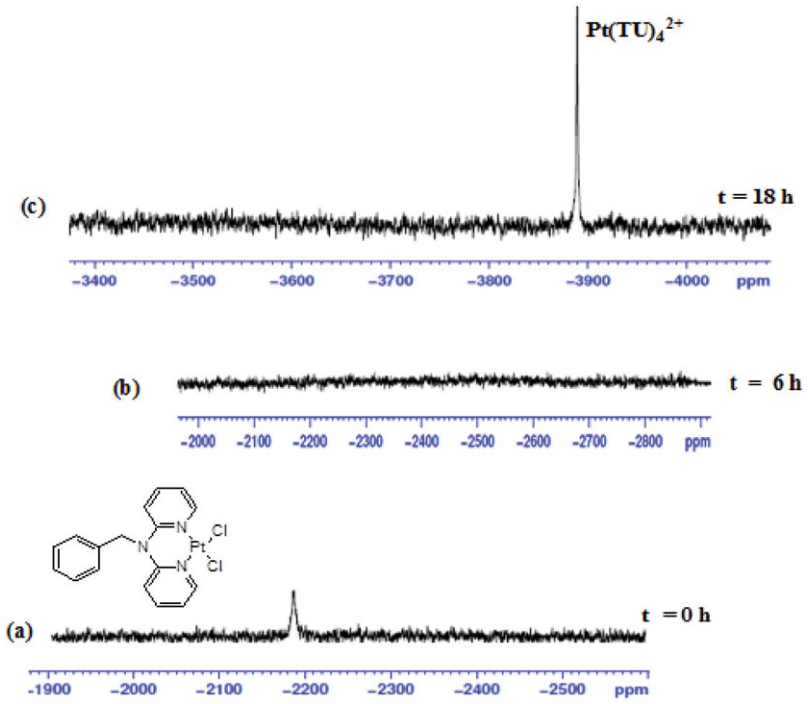

Figure 9 (a) Time-dependent ^{195}Pt NMR chemical shift of Pt2 in DMF-d_7 showing a peak at −2189.2 ppm. (b) Addition of 6 equiv. of TU leads to the disappearance of the peak at −2189.2 ppm. (c) The peak at −3889.2 ppm is attributed to the formation of the [Pt(TU)$_4$$^{2+}$] complex. [Color figure can be viewed at wileyonlinelibrary.com]

is larger than that of Pt2 (129.63°) that results in a more effective collisions between the metal and the nucleophile.

Introduction of a second platinum center in Pt2 to form a dinuclear Pt(II) complex leads to structural and conformational differences that influence their chemical reactivity. This difference in the three dinuclear complexes is aided by the incorporation of an aminomethyl spacer that provides greater flexibility to the complexes. This results in the twisting of complexes to form cavities of different shapes and sizes. The inorganic hybrid architectures show novel chemical and physical properties of the investigated dinuclear Pt(II) complexes.

The reactivity of the dinuclear complexes is approximately 100 times slower than the mononuclear complexes. The reactivity trend can be summed up as Pt4 (meta) > Pt3 (ortho) > Pt5 (para) even though the reactivities are small. In these complexes, there are two types of cavities which influence the reactivity. These are the cavity due to the twisting of the two pyridine rings attached to the Pt-atoms and the cavity created due to the formation of the dinuclear complex. The first cavity is measured by determining the basal angle as shown in Fig. 2 and values presented in Table III. The basal angle shows that Pt4 to have the smallest angle compared to Pt3 and Pt5 which are comparable. One would therefore expect the cavity in Pt4 to entrap the incoming nucleophile much better than Pt3 and Pt5 resulting in higher reactivity, which is in agreement with the observed results. Looking at the bowl-like cavity between the two Pt-metal centers, it can be noted that the ─CH_2─ and the phenyl that form the pendant attachment introduce steric hindrance at a different degree to each complex on both side of the platinum atom. For instance, the twisting of pyridyl rings in Pt5 causes the coordinated metal ions to be maximally shielded and thus prevented from nucleophilic attack. This is very different to the mononuclear complexes that do not experience this type of steric hindrance and therefore accounting for the difference in reactivity between the two types of systems.

The shape and size of these cavities also influence the effectiveness of the entrapment of the incoming nucleophile exhibiting the difference in reactivity [56,57]. The DFT data show that the electronic effect of all the three dinuclear complexes is very similar, suggesting that the difference in reactivity is mostly due to the structural conformation [58]. This is in agreement with previous studies [58] showing the bridging linker to confer special structural properties on the metal complexes that controls their reactivity and stability.

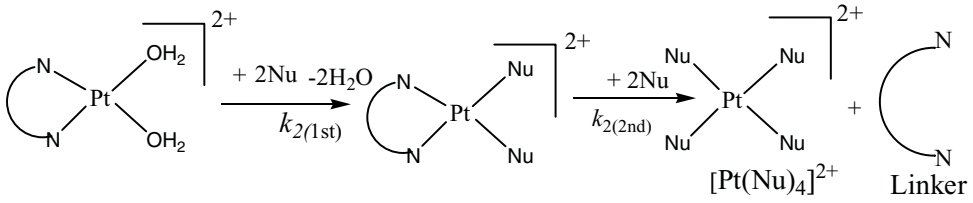

Scheme 3 Proposed substitution mechanism showing simultaneous substitution of diaqua ligands with nucleophiles (Nu) on Pt2 followed by ring opening of the ligand.

Table IV A Summary of the Second Order Rate Constants, k_2, for the Simultaneous Substitution of Aqua Ligands ($k_{2(1st)}$) and the Dechelation Step $k_{2(2nd)}$ at pH = 2.0, T = 298.15 K, I = 0.1 M $NaClO_4$

		Second-Order Rate Constant ($M^{-1}s^{-1}$)	
Complex	Nu	$k_{2(1st)}$	$k_{2(2nd)} \times 10^{-3}$
Pt1	TU	28.85 ± 0.18	20 ± 3
	DMTU	33.42 ± 0.15	10 ± 1
	TMTU	10.38 ± 0.05	10 ± 1
Pt2	TU	33.34 ± 0.27	30 ± 4
	DMTU	25.09 ± 0.19	10 ± 0.1
	TMTU	11.45 ± 0.04	10 ± 0.2
Pt3	TU	0.08 ± 0.001	1 ± 0.03
	DMTU	0.02 ± 0.001	1 ± 0.01
	TMTU	0.01 ± 0.001	1 ± 0.01
Pt4	TU	0.16 ± 0.004	40 ± 2
	DMTU	0.21 ± 0.003	20 ± 1
	TMTU	0.04 ± 0.002	10 ± 1
Pt5	TU	0.04 ± 0.001	3 ± 0.06
	DMTU	0.01 ± 0.001	1 ± 0.01

Note: Reaction of **TMTU** with **Pt5** was too slow.

Investigation of structural differences in dinuclear Pt(II) complexes shows steric effect of the spacer through cavities realized through changing the anchorage position, which supports previous study by Mambanda and Jaganyi [58]. This study shows the dinuclear complexes to have a cage effect through adopting bowl-shaped molecular structures that controls reactivity. The decrease in the rate of substitution of dinuclear complexes is attributed to steric contributions imposed by the cavities of the complexes to varying degrees as shown by the different size and shape of cavities as shown by Figs. S34 and S35 (in the Supporting Information). The data obtained in this study support the previous studies by Jaganyi and group [58] that subtle differences in the structural makeup of the linker can have a greater influence on the reactivity of dinuclear Pt(II) complexes. In contrast to previous studies where metal–metal distance has an influence on the reactivity of dinuclear complexes, this paper reports reactivity to be mainly dependent on conformational makeup and to smaller extent electronic contribution in the ortho, meta, and para complexes to varying levels. Thus, the stability of the complexes was maximized when steric and electronic parameters reinforced each other.

The substitution of the aqua ligands by nucleophiles TU, DMTU, and TMTU showed a clear dependence on the steric hindrance of the nucleophile. However, in Pt1 and Pt4 DMTU was found to be slightly faster than TU; this enhanced reactivity is attributed to the inductive effect introduced by the two methyl groups on DMTU which over compensates the steric effect [59]. The small but positive enthalpy and large negative entropy confirm the associative mode of mechanism for all the investigated complexes. This is an indication that the mechanistic reactions of these complexes are characterized by bond formation in the transition state [60,61]. The activation parameters also imply a good degree of ligand participation in the transition state and a more compact transition state than that of the starting reactants [62].

CONCLUSION

The substitution kinetics of mono- and dinuclear Pt(II) complexes with 2,2′-dipyridylamine units connected by the alkyl–phenyl spacer was investigated. The results show that upon coordination of the metal atoms to the pyridyl rings of 2,2′-dipyridylamine the complex adopts inclined planes with varying dihedral and basal angles. When the two metals are joined together through a bridging ligand, the dinuclear complexes form bowl-like cavities whose shape and size are very dependent on the position to which the phenyl moiety is joined to the complex. The study has shown that the reactivities of these complexes are controlled by steric effect, which is due to the architectural framework of the complexes. The mononuclear complexes being less sterically hindered compared to the dinuclear complexes, as such are 100 times more reactive. The cavities formed due to the presence of the

Table V A Summary of the Activation Parameters for the Simultaneous Substitution of Aqua Ligands and the Dechelation Step of the Studied Pt(II) Complexes

		Activation Enthalpy (kJ mol^{-1})		Activation Entropy (J K^{-1} mol^{-1})	
Complex	Nu	$\Delta H_1^{\#}$	$\Delta S_1^{\#}$	$\Delta H_2^{\#}$	$\Delta S_2^{\#}$
Pt1	TU	33.78 ± 0.6	-143 ± 2	22.27 ± 0.6	-246 ± 2
	DMTU	33.19 ± 1.8	-144 ± 6	22.60 ± 0.9	-254 ± 3
	TMTU	44.39 ± 1.0	-115 ± 3	60.76 ± 3.5	-112 ± 12
Pt2	TU	39.81 ± 0.3	-121 ± 1	20.54 ± 0.8	-249 ± 2
	DMTU	43.47 ± 1.7	-111 ± 5	26.74 ± 0.9	-241 ± 3
	TMTU	40.86 ± 0.8	-126 ± 3	41.02 ± 1.5	-179 ± 5
Pt3	TU	29.17 ± 0.5	-192 ± 2	16.78 ± 0.1	-266 ± 1
	DMTU	26.37 ± 0.5	-229 ± 2	12.48 ± 0.3	-291 ± 1
	TMTU	39.03 ± 0.3	-183 ± 1	20.14 ± 0.1	-255 ± 1
Pt4	TU	19.07 ± 0.3	-226 ± 1	35.31 ± 0.9	-181 ± 3
	DMTU	26.83 ± 0.6	-201 ± 2	27.49 ± 0.6	-221 ± 2
	TMTU	33.52 ± 0.2	-191 ± 1	31.05 ± 1.1	-209 ± 4
Pt5	TU	32.25 ± 1.4	-193 ± 4	20.63 ± 0.6	-260 ± 2
	DMTU	37.00 ± 0.7	-196 ± 2	32.52 ± 0.6	-225 ± 2

pyridine rings, and the —CH_2— and phenyl group as the linker plays a big role in influencing the entrapment of the incoming nucleophile which in turn controls the reactivity of these complexes.

The substitution behavior of all the complexes followed a two-step substitution reaction where the first step is the simultaneous displacement of all the aqua ligands, whereas the second step is a dechelation process. The activation parameters confirmed the mode of mechanism to be associative in nature. The displacement of the linker following coordination of excess nucleophile to the congested platinum(II) center suggests a possibility of instability of the system which could limit its application as an anticancer agent. The study for the first time has provided an insight into how multiple substitutions; in this case, four aqua ligands are substituted by biological nucleophiles. These results suggest that tuning the geometric structure may be an effective molecular design strategy toward potent anticancer agents. The knowledge generated has provided a better understanding of the interactions of these Pt(II) complexes with nitrogen and sulfur-containing biomolecules and is likely to assist in the development of new platinum-based anticancer agents with improved efficacy.

The author gratefully acknowledges the support from the University of Kwazulu Natal. I am also grateful to Mr. Craig Grimmer and Miss Janse van Resenburg for NMR, mass, and elemental analyses.

BIBLIOGRAPHY

1. Lippert, B. Cisplatin. Chemistry and Biochemistry of a Leading Anti-cancer Drug; Wiley-VCH: Weinheim, Germany, 1999; pp. 3–27.
2. Farrell, N. Transition Metal Complexes as Drug and Chemotherapeutic Agents; Kluwer: Dordrecht, the Netherlands; 1989; pp. 8–30, 46–54.
3. Fekl, U.; Goldberg, K. I. Adv Inorg Chem 2003, 54, 260–270.
4. Reedijk, J. Chem Rev 1999, 99, 2499–2510.
5. Brabec, V.; Kasparkova, J. Drug Resist Updat 2005, 8, 131–146.
6. Wong, E.; Giandomenico, C. M. Chem Rev 1999, 99, 2451–2466.
7. (a) Jaganyi, D.; Reddy, D.; Gertenbach, J. A.; Hofmann, A.; van Eldik, R. J Chem Soc, Dalton Trans 2004, 2, 299–304; (b) Jaganyi, D.; Hofmann, A.; van Eldik, R. Angew Chem, Int Ed 2001, 40, 1680–1683.
8. Hofmann, A.; Jaganyi, D.; Munro, O. Q.; Liehr, G.; van Eldik, R. Inorg Chem 2003, 42, 1688–1700.
9. Atwood, J. D. Inorganic and Organometallic Reaction Mechanisms, 2nd ed.; Wiley-VCH: New York, 1997; pp. 43–61; Atwood, J. D. Inorganic Organometallic Reaction Mechanisms; Brook/Cole: Monterey, CA, 1985; pp. 82–83.
10. Wilkins, R. G. Kinetics and Mechanism of Reactions Transition Metal Complexes, 2nd edn; Wiley-VCH: Weinheim, Germany, 1991; pp. 199–201, 221–242.
11. Giuseppe, A.; Giuseppe, B.; Santo, L.; Domenico, M.; Raffaello, R.; Tobe, L. M. Inorg Chem 1987, 26, 185–190.
12. Boulikas, T.; Pantos, A.; Bellis, E.; Christofis, P. Cancer Ther 2007, 5, 537–583.

13. Wheate, N. J.; Collins, J. G. Coord Chem Rev 2003, 241, 133–145.
14. Olszewski, U.; Hamilton, G. Med Chem 2010, 10, 293–301.
15. El-Sherif, A. A.; Shoukry, M. M. Inorg Chim Acta 2007, 360, 473–487.
16. Barry, M. A.; Behnke, A. C.; Eastman, A. Biochem Pharm 1990, 40, 2353–2362.
17. Lokich, J. Cancer Invest 2001, 19, 756–760.
18. Shibata, S.; Ochi, A.; Mori, K. Neurol Med Chir 1990, 30, 242–245.
19. Soldatović, T.; Bugarčić, Ž. D.; van Eldik, R. Dalton Trans 2009, 4526–4532.
20. Ertürk, H.; Magut, J.; Puchta, R.; van Eldik, R. Dalton Trans 2008, 2759–2766.
21. Hall, M. D.; Hambley, T. W. Coord Chem Rev 2002, 232, 49–56.
22. Farrell, N.; Qu, Y.; Hacker, M. P. J Med Chem 1990, 33(8), 2179–2184.
23. Farrell, N.; Appleton, T. G.; Qu, Y.; Roberts, J. D.; Soares-Fontes, A. P.; Skov, K. A.; Wu, P.; Zou, Y. Biochemistry 1995, 34, 15480–15486.
24. Jaganyi, D.; Munisamy, V. M.; Reddy, D. Int J Chem Kinet 38, 202–210.
25. Hofmann, A.; van Eldik, R. J Chem Soc, Dalton Trans 2003, 2979–2985.
26. Cox, J. W.; Berners-Price, S. J.; Davies, M. S.; Barlage, W.; Qu, Y.; Farrell, N. Inorg Chem 2000, 39, 1710–1709.
27. Banerjee, T.; Dubey, P.; Mukhopadhyay, R. Biochimie 2012, 94, 494–502.
28. Malina, J.; Kasparkova, J.; Farrell, N.; Brabec, V. Nucleic Acids Res 2010, 1–9.
29. (a) Guilard, R.; Kadish, K. M. Chem Rev 1988, 88, 1121–1146; (b) Brown, D. G.; Byers, P. K.; Canty, A. J. Organometallics 1990, 9, 1231–1235; (c) Canty, A. J. Acc Chem Res 1992, 25, 83–90.
30. Sauvageot, E.; Marion, R.; Sguerra, F.; Grimault, A.; Daniellou, R.; Hamel, M.; Gaillard, S.; Renaud, J. Org Chem Front 2014, 1, 639–644.
31. Ashby, M. T. Comments Inorg Chem 1990, 10, 297–313.
32. (a) Curtis, W. E.; Muldrow, M. E.; Parker, N.; Barkley, B. R.; Linas, S. L.; Repine, J. E. Proc Natl Acad Sci U S A 1988, 85, 3422–3425; (b) Sprong, R. C.; Aarsman, C. J. M.; van Oirschot, J. F. L. M.; van Asbeck, B. S. J Lab Med 1997, 129, 470–481.
33. (a) De Agazio, M.; Zacchini, M. Plant Cell Environ. 2001, 24, 237–244; (b) Matsumoto, K.; Aizawa, H.; Inoue, H.; Koto, H.; Fukuyama, S.; Hara, N. Eur. J. Pharmacol. 2000, 403, 157–161.
34. Bianca, A.; Bray, D. J.; Clegg, J. K.; Gloe, K.; Karsten, G.; Kataeva, O.; Lindoy, F. L.; McMurtrie, J. C.; Steel, P. J.; Sumby, C. J.; Wenzel, M. Dalton Trans 2006, 4783–4794.
35. (a) Fakih, S.; Tung, W. C.; Eierhoff, D.; Mock, C.; Krebs, B. Z. Anorg Allg Chem 2005, 631, 1397–1402; (b) Rauterkus, M. J.; Fakih, S.; Mock, C.; Krebs, I. P. Inorg Chim Acta 2003, 350, 355–365.
36. (a) Bogojeski, J.; Bugarčić, Ž. D.; Puchta, R.; van Eldik, R. Eur J Inorg Chem 2010, 5439–5445; (b) Jovanović, S.; Petrović, B.; Čanović, D.; Bugarčić, Ž. D. Int J Chem Kinet 2011, 43, 99–106; (c) Hochreuther, N.; Nandibewoor, S. T.; Puchta, R.; van Eldik, R. Dalton Trans 2012, 41, 512–522; (d) Summa, W.; Schiessl, R.; Puchta, N.; van Eikema, H.; van Eldik, R; R. Inorg Chem 2006, 45, 2948–2959.
37. Origin7.5TM v7.5714 (B5714); Origin Lab Corporation: Northampton, MA, 2003.
38. Schiessl, W. C.; Summa, N. K.; Weber, C. F.; Gubo, S.; Duecker-Benfer, C.; Puchta, R.; van Eikema, H.; van Eldik, R. Z. Anorg Allg Chem 2005, 631, 2812–2819.
39. Frisch, M. J.; Trucks, G. W.; Schlegel, H. B.; Scuseria, G. E.; Robb, M. A.; Cheeseman, J. R.; Scalmani, G.; Barone, V.; Mennucci, B.; Petersson, G. A.; Nakatsuji, H.; Caricato, M.; Li, X.; Hratchian, H. P.; Izmaylov, A. F.; Bloino, J.; Zheng, G.; Sonnenberg, J. L.; Hada, M.; Ehara, M.; Toyota, K.; Fukuda, R.; Hasegawa, J.; Ishida, M.; Nakajima, T.; Honda, Y.; Kitao, O.; Nakai, H.; Vreven, T.; Montgomery, J. A., Jr., Peralta, J. E.; Ogliaro, F.; Bearpark, M.; Heyd, J. J.; Brothers, E.; Kudin, K. N.; Staroverov, V. N.; Kobayashi, R.; Normand, J.; Raghavachari, K.; Rendell, A.; Burant, J. C.; Iyengar, S. S.; Tomasi, J.; Cossi, M.; Rega, N.; Millam, J. M.; Klene, M.; Knox, J. E.; Cross, J. B.; Bakken, V.; Adamo, C.; Jaramillo, J.; Gomperts, R.; Stratmann, R. E.; Yazyev, O.; Austin, A. J.; Cammi, R.; Pomelli, C.; Ochterski, J. W.; Martin, R. L.; Morokuma, K.; Zakrzewski, V. G.; Voth, G. A.; Salvador, P.; Dannenberg, J. J.; Dapprich, S.; Daniels, A. D.; Farkas, O.; Foresman, J. B.; Ortiz, J. V.; Cioslowski, J.; Fox, D. J.; Gaussian 09, Revision A.1; Gaussian: Wallingford, CT, 2009.
40. (a) Becke, A. D. J Chem Phys 1993, 98, 1372–1384, 5648–5642; (b) Lee, C.; Yang, W.; Parr, R. G. Phys Rev B 1988, 37, 785–795; (c) Stephens, P. J.; Devlin, F. J.; Chabalowski, C. F.; Frisch, M. J. J Phys Chem 1994, 98, 1623–1627; (d) Miehlich, B.; Savin, A.; Stoll, H.; Preuss, H. Chem Phys Lett 1989, 157, 200–206.
41. (a) Huang, Y.; Zhang, M.; Ye, L.; Guo, X.; Han, C. C.; Li, Y.; Hou, J. J Mater Chem 2012, 22, 5700–5705; (b) Rogers, M. T. J Phys Chem, Sect A 2001, 105, 2374–2383; (c) Bratislav, Ž. J.; Aleksandar, D. M.; Željko, V.; Ivan, O. J. J Serb Chem Soc 2007, 72, 1191–1200; (d) Kinunda, G.; Jaganyi, D. Transition Met Chem 2016, 41, 235–248.
42. (a) Gornitzka, H.; Stalke, D. Organometallics 1994, 13, 4398–4405; (b) Wekesa, I. M.; Jaganyi, D. Dalton Trans 2014, 43, 2549–2558.
43. (a) Parr, R. G.; Yang, W.; Density Functional Theory of Atoms and Molecules; Oxford University Press: New York, 1989; pp. 3–350; (b) Chattaraj, P. K.; Giri, S. Annu Rep Prog Chem, Sect C: Phys Chem 2009, 105, 13–39; (c) Chattaraj, P. K.; Chemical Reactivity Theory: A Density Functional View; Taylor & Francis/CRC Press: Boca Raton, FL, 2009; pp 109–112.

44. Pearson, R. G.; Chemical Hardness–Applications from Molecules to Solids; VCH Wiley: Weinheim, Germany, 1997; pp. 27–63.
45. Chattaraj, P. K. J Chem Sci 2005, 117, 561–571; special issue on chemical reactivity.
46. Geerlings, P.; De Proft, F.; Langenaeker, W. Chem Rev 2003, 103, 1793–1873.
47. (a) Parr, R. G.; Szentpaly, L. V.; Liu, S. J Am Chem Soc 1999, 121, 1922–1924; (b) Chattaraj, P. K.; Sarkar, U.; Roy, D. R. Chem Rev 2006, 106, 2065–2091.
48. Ram, K. R.; Soumen, S. Annu Rep Prog Chem, Sect C 2010, 106, 118–162.
49. (a) Sen, K. D.; Mingos, D. M. P. Struct Bonding: Chemical Hardness 1993, 80, 103–108; (b) Parr, R. G.; Pearson, R. G. J Am Chem Soc 1983, 105, 7512–7516; (c) Pearson, R. G. Chemical Hardness: Applications from Molecules to Solids; Wiley-VCH: Weinheim, Germany, 1997; pp. 12–33.
50. Still, B. M.; Kumar, P. G. A.; Aldrich-Wright, J. R.; Price, W. S. Chem Soc Rev 2007, 36, 665–686.
51. Ongoma, P. O.; Jaganyi, D. Dalton Trans 2013, 42, 2724–2734.
52. Ongoma, P. O.; Jaganyi, D. Transition Met Chem 2014, 39, 407–420.
53. Shoukry, A. A. J Chem Sci 2013, 125, 643–651.
54. Adnan, S. A.; Mika, K. Curr Med Chem 2006, 13, 1337–1357.
55. (a) Tobe, M. L.; In Comprehensive Coordination Chemistry; Wilkinson, G., Ed.; Pergamon Press: Oxford, UK, 1987; Vol. 1, pp. 311–329; (b) Basolo, F.; Pearson, R. G.; Mechanisms of Inorganic Reactions; Wiley: New York, 1968; pp. 299–354; (c) Langford, C. H.; Gray, H. B.; Ligand Substitution Processes; W. A. Benjamin: New York, 1965; pp. 20–28, 43–65; (d) Basolo, F. Coord Chem Rev 1996, 154, 151–161.
56. Jodrell, D. I.; Evans, T. R. J.; Steward, W.; Cameron, D.; Prendiville, J.; Aschele, C.; Noberasco, C.; Lind, M.; Carmichael, J.; Dobbs, N.; Camboni, G.; Gatti, B.; Braud De, F. Eur J Cancer 2004, 40, 1872–1877.
57. (a) Sakaki, S.; Biswas, B.; Sugimoto, M. J Chem Soc, Dalton Trans 1997, 803–809; Su, M. D.; Chu, S. Inorg Chem 1988, 37, 3400–3406; (b) Kozuch, S.; Amatore, C.; Jutand, A.; Shaik, S. Organometallics. 2005, 24, 2319–2330.
58. Mambanda, A.; Jaganyi, D. Dalton Trans 2012, 41, 908–920.
59. Jaganyi, D.; Tiba, F.; Munro, O. Q.; Petrović, B.; Bugarcić, Ž. D. Dalton Trans 2006, 24, 2943–2949.
60. Ertürk, H.; Hofmann, A.; Puchta, R.; van Eldik, R. Dalton Trans 2007, 2295–2301.
61. Mandal, A.; Karmakar, P.; Mallick, S.; Bera, B. K.; Mondal, S.; Ray, S.; Ghosh, A. K. J Chem Sci 2012, 124, 801–807.
62. Bera, B. K.; Ray, S.; Mondal, S.; Karmakar, P.; Mandal, A.; Mallick, S.; Ghosh, A. K. J Chem 2013, 42, 441–458.